Inorganic Chemistry
Cite This: Inorg. Chem. 2018, 57, 15474−15480
Article
pubs.acs.org/IC

Inverse Design of a Catalyst for Aqueous CO/CO_2 Conversion Informed by the Ni^{II}−Iminothiolate Complex

Alexander M. Chang, Benjamin Rudshteyn, Ingolf Warnke, and Victor S. Batista*

Department of Chemistry and Energy Sciences Institute, Yale University, New Haven, Connecticut 06520, United States

Supporting Information

ABSTRACT: A computational inverse design method suitable to assist the development and optimization of molecular catalysts is introduced. Catalysts are obtained by continuous optimization of "alchemical" candidates in the vicinity of a reference catalyst with well-defined reaction intermediates and rate-limiting step. A Ni^{II}−iminoalkoxylate catalyst for aqueous CO/CO_2 conversion is found with improved performance relative to a Ni^{II}−iminothiolate reference complex, previously reported as a biomimetic synthetic model of CO dehydroxygenase. Similar energies of other intermediates and transition states along the reaction mechanism show improved scaling relations relative to the reference catalyst. The linear combination of atomic potential tight-binding model Hamiltonian and the limited search of synthetically viable changes in the reference structure enable efficient minimization of the energy barrier for the rate-limiting step (i.e., formation of $[LNi^{II}(COOH)]^-$), bypassing the exponential scaling problem of high-throughput screening techniques. The reported findings demonstrate an inverse design method that could also be implemented with multiple descriptors, including reaction barriers and thermodynamic parameters for reversible reactivity.

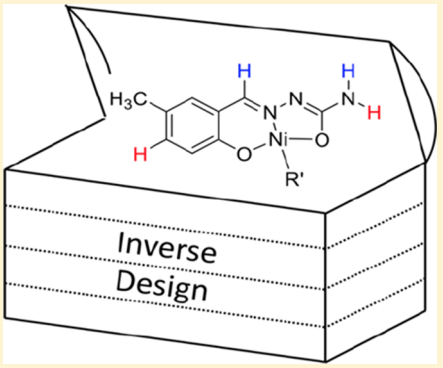

1. INTRODUCTION

The development of computational tools to assist the development and optimization of catalysts could greatly benefit various areas of research in both industry and academia.[1] Here, we introduce an inverse design (ID) methodology tailored for the rational design of catalysts based on a reference complex and the energy barrier for the rate-limiting step of the catalytic cycle. The method builds on our previously developed gradient-assisted deterministic search algorithm, which operates on landscapes of continuous "alchemical" frameworks described by a tight-binding (TB) linear combination of atomic potential (LCAP) Hamiltonian.[2] We exploit the advantages of the LCAP approach when compared to brute-force high-throughput, including the computational cost of expectation values, which is polynomial in the number of basis functions, and the availability of genetic or gradient-assisted search algorithms for local optimization.

The search of catalysts exhibiting selective and efficient reactivities is challenging.[1] Design strategies based on "guess-and-check" approaches and exhaustive enumeration quickly become ineffective due to the exponentially large number of possibilities and the computational time required for the evaluation of individual candidates. ID algorithms[3−12] circumvent exhaustive enumeration by searching for structures through discrete[3] or continuous[5,6] transformations aimed at identifying a local or global minimum with suitable properties. Earlier ID studies were directed at finding solids with maximal band gaps, using a simulated annealing algorithm and searching in a discrete space of atomic superlattices,[3] and a genetic algorithm to search for quaternary semiconductors with defined band gaps.[13,14]

The computational efficiency of LCAP approaches is greatly enhanced as gradient-assisted optimization algorithms can be employed to identify local minima as applied toward the search for molecules with optimized polarizabilities and hyperpolarizabilities.[15] To enhance the computational efficiency and enable large libraries, the LCAP method was implemented at the TB Hückel level and proved to be effective at locating optimized structures within large libraries of 10^2 to 10^6 structures.[15] The LCAP approach has also been combined with gradient-directed Monte Carlo (GDMC) jumps, which allow the search algorithm to cross barriers and escape when trapped in local minima.[16,17] The GDMC method was used to optimize highest occupied molecular orbital−lowest unoccupied molecular orbital transitions,[17] in protein sequence design,[4] and to study protein folding.[18]

Recently, we generalized the TB-LCAP approach[15] and applied it toward optimizing photoabsorption properties of organic adsorbates for photocatalytic applications.[2] The extended-Hückel (EH) formalism utilizes s, p, and d atomic orbitals and thus enables description of the full valence shell for a wide range of molecular systems. Here, we use the EH TB-LCAP approach to search for catalysts with improved reactivity relative to a reference complex. We develop a parallelized algorithm that efficiently screens for structures that

Received: October 1, 2018
Published: November 27, 2018

DOI: 10.1021/acs.inorgchem.8b02799
Inorg. Chem. 2018, 57, 15474−15480

minimize the energy difference between two intermediate structures corresponding to the reactant and the transition state of the rate-limiting step of the reaction. For the first time, an ID application tailored to assist the development of a catalyst for CO/CO_2 conversion is reported. With this ID, we can screen for the molecules with the smallest energy differences and evaluate them further at higher levels of theory.

Ligand ID is applied to improve upon performance of a Ni^{II}–iminothiolate catalyst for CO/CO_2 conversion. The workflow is organized, as follows: (i) the ID algorithm is applied to identify ligands of promising complexes that could exhibit a lower energy barrier for the rate-limiting step; (ii) the free energy profile for the proposed catalyst is compared to that of the original.

CO/CO_2 conversion is a central process in carbon metabolism in biology and in industrial applications, including H_2 production by the water–gas shift reaction.[19] Carbon monoxide dehydrogenase (CODH) is a natural enzyme with a Ni active center that catalyzes reversible CO/CO_2 interconversion to provide electrons needed by other metabolic steps.[20−22] Crabtree and co-workers[23,24] proposed a Ni^{II}–iminothiolate catalyst (Figure 1), as a functional biomimetic

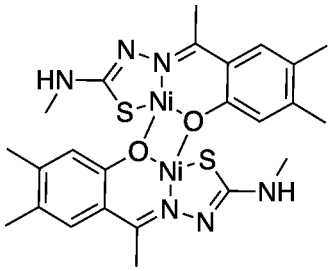

Figure 1. Dimer of the Ni^{II}–iminothiolate complex, proposed as a functional model for CO dehydrogenase by Lu and Crabtree.[23]

CODH model system. Their Ni^{II}-complex engages in CO/CO_2 conversion driven by the oxidizing agent methylviologen (mv^{2+}) and produces protons under aqueous conditions with acetate at room temperature, as follows

$$CO + H_2O + 2AcO^- + 2mv^{2+} \rightarrow CO_2 + 2AcOH + 2mv^+ \quad (1)$$

The proposed Ni catalyst mimics the thiolate environment in CODH, which softens the metal center and enhances its ability to bind CO. However, thiolate ligands tend to form disulfide bridges which inactivate the catalyst and prevent CO from binding to the catalytic site. The iminothiolate ligand has been shown to reduce the tendency for dimerization in polar aqueous environments while maintaining the electron-donating properties of the thiolate ligand.[25]

The postulated catalytic mechanism[26] is consistent with available kinetic data, similar to the well-known water–gas shift reaction[19]

$$CO(g) + H_2O(l) \rightarrow CO_2(g) + H_2(g) \quad (2)$$

Upon binding to a redox active metal center, the CO becomes activated for a nucleophilic attack by water to produce a metalcarboxylic acid intermediate (M–COOH), which undergoes decarboxylation to produce a metal hydride, subsequently protonated to evolve H_2. However, H_2 evolution is not observed in the Ni^{II}–iminothiolate catalytic cycle, which can be explained by assuming that upon formation of the Ni–CO bond and nucleophilic water attack, the metal–carboxylic acid deprotonates. Deprotonation is consistent with the observed pH-dependent reaction rates. Decarboxylation is induced through the oxidation of $Ni–COO^-$ by mv^{2+}.[23]

We have reported a detailed ab initio mechanistic study to analyze the catalytic reaction pathway, including a complete analysis of the reaction energy profile and energy barrier for the rate-limiting step.[26] We found that the mechanism is as follows: (i) the dimer is cleaved by water to form the active monomer species; (ii) the water ligand is exchanged by CO; (iii) a water nucleophilic attack and subsequent deprotonation forms a Ni^{II} carboxylic acid species during the rate-limiting step; (iv) proton transfer followed by electron transfer forms a Ni^{I} carboxylate; (v) a water nucleophilic attack forms a five-coordinate Ni^{I} species; (vi) electron transfer and loss of CO_2 reforms the active species.

In this report, we display a proof of concept of our new ID algorithm by generating an improved ligand set for the Ni^{II} complex with a lower barrier for the rate-limiting step, as verified by density functional theory (DFT), while keeping other steps in the mechanism mostly unaffected. The method is widely applicable to other catalytic systems or implemented with multiple descriptors, including reaction barriers and thermodynamic parameters for reversible reactivity.

2. METHODS

2.1. TB-LCAP Hamiltonian. We outline the use of the EH TB method for fast screening according to the LCAP followed by DFT assessment of the identified structures.[2] EH calculations provide valuable qualitative description of molecular orbitals and have been extensively applied to simulate a wide range of systems, including photoabsorption spectra of molecular and solid state structures,[27,28] and interfacial electron transfer occurring in sensitized TiO_2 surfaces.[29−33]

The EH Hamiltonian **H** is defined in terms of empirical atomic potentials and a set of Slater-type atomic orbitals (STOs). Eigenstates are found by solving the eigenvalue problem defined by the time-independent Schrödinger equation

$$\hat{H}\hat{Q} = E\hat{S}\hat{Q} \quad (3)$$

which is solved by diagonalization. In eq 3, **Q** represents the matrix of coefficients of molecular orbitals in the basis of STOs, **E** is the molecular orbital energies, and **S** is the overlap matrix of the nonorthogonal STOs.

In the EH/TB-LCAP approach, we introduce a set of participation coefficients $b_i^{(A)}$ allowing for a superposition of atom or functional group types (A) on atomic sites (i). For a given site j, the weights define the *alchemical* composition allowing for a continuous transformation of atom or functional group types during the ID-optimization. The diagonal elements of **H** are weighted averages of EH Hamiltonian elements of all atom types (A) considered for site i, as follows

$$H_{i\alpha,i\alpha} = \sum_{A=1}^{N_i} b_i^{(A)} h_{i\alpha,i\alpha}^{(A)} \quad (4)$$

where $b_i^{(A)}$ represents the coefficient for an atomic orbital of atom type A at site i, N_i is the number of atom types considered for site i, and $h_{i\alpha,i\alpha}^{(A)}$ is the EH Hamiltonian matrix element for atom type A at site i. The off-diagonal elements of **H** are given analogously, as follows

$$H_{i\alpha,j\beta} = \sum_{A'=1}^{N_j} b_j^{(A')} \sum_{A=1}^{N_i} b_i^{(A)} h_{i\alpha,j\beta}^{(A,A')} \quad (5)$$

DOI: 10.1021/acs.inorgchem.8b02799
Inorg. Chem. 2018, 57, 15474−15480

with atomic orbitals belonging to atom type A' at site j and A at site i. For a pair of atom types A and A' at sites i and j, the off-diagonal Hamiltonian elements are defined as

$$h_{i\alpha,j\beta}^{(A,A')} = \frac{1}{2}K' S_{i\alpha,j\beta}^{(A,A')}(h_{i\alpha,i\alpha}^{(A)} + h_{j\beta,j\beta}^{(A')}) \quad (6)$$

where K' is defined by the Wolfsberg-Helmholtz formula[34]

$$K' = 1.75 + \left(\frac{h_{i\alpha,i\alpha}^{(A)} - h_{j\beta,j\beta}^{(A')}}{h_{i\alpha,i\alpha}^{(A)} + h_{j\beta,j\beta}^{(A')}}\right)^2 - 0.75\left(\frac{h_{i\alpha,i\alpha}^{(A)} - h_{j\beta,j\beta}^{(A')}}{h_{i\alpha,i\alpha}^{(A)} + h_{j\beta,j\beta}^{(A')}}\right)^4 \quad (7)$$

The off-diagonal overlap matrix elements are

$$S_{i\alpha,j\beta} = \sum_{A'=1}^{N_j} b_j^{(A')} \sum_{A=1}^{N_i} b_j^{(A)} S_{i\alpha,j\beta}^{(A,A')} \quad (8)$$

Equations 4 and 5 define the Hamiltonian of an arbitrary alchemical intermediate structure. Diagonalization and computation of expectation values allow for continuous variation relative to the participation coefficients $b_i^{(A)}$ that define the chemical composition. Gradient-based methods are used to perform local optimization of the composition relative to the property of interest. Because the local minimum does not generally correspond to chemical structures with pure atomic types, the participation coefficients have to be rounded off to the closest structure with pure atomic types and subsequently analyzed at the DFT level. Given an initial, randomized set of participation coefficients, the algorithm propagates them to their closest local minimum while the global minimum is searched for by many local optimizations initialized using randomized initial conditions.

2.2. TB-LCAP Optimization of Energy Differences. We generalize the TB-LCAP approach for catalyst design by evaluating an objective function that corresponds to the energy difference (ΔE) associated with the activation energy barrier for the rate-limiting step of the reaction mechanism. Specifically, after identifying the rate-determining step in a catalytic cycle via DFT analysis, the newly implemented objective function is used to locate catalysts that minimize the electronic energy barrier of that reaction step. Subsequently, the geometries and energies of the most promising candidates are refined using DFT and the entire catalytic cycle is analyzed based on the DFT-optimized geometries, energies, and free energies. A schematic representation of the ID algorithm is shown in Figure 2.

2.3. Density Functional Calculations. We employ DFT[35−37] calculations to identify and characterize the lowest energy intermediates for each step of the catalytic cycle using the same methods as in our previous paper.[26] Briefly, we used the well-established B3LYP hybrid density functional, including Becke's three parameter exchange[38] and the Lee, Yang, and Parr correlation,[39] as implemented in Gaussian 09, Revision D.01.[40] For geometry optimization and thermal/entropic corrections (T = 298.15 K),[41] we used the Def2SVP basis set[42] for nonoxygen elements and 6-31+G(d,p) basis set for oxygen.[43,44] For the single-point energy, we used the Def2TZVP basis set[42] and the 6-311+G(d,p) basis set for oxygen.[44,45] All calculations were done in a dielectric continuum of methanol (one of the experimental solvents)[23] provided by the SMD model,[46] together with default optimization criteria and integration grids. The free energies are corrected for the different standard state in solution (1 M) versus that in the calculations by default (1 atm) by +1.89 kcal/mol for every extra product or −1.89 kcal/mol for every extra reactant.[47,48] Rate-determining transition states for the complexes with new ligand sets were identified. Relaxed scans (fully relaxing all coordinates but the coordinate of interest during scanning of the H_2O−CO distance) were used to prepare optimal guess geometries for the transition state, after which the actual transition state optimizations, which led to relevant lone imaginary frequencies, were performed.

2.4. Turnover Frequency Calculations. The turnover frequencies of the catalysts were estimated using the Eyring equation[49]

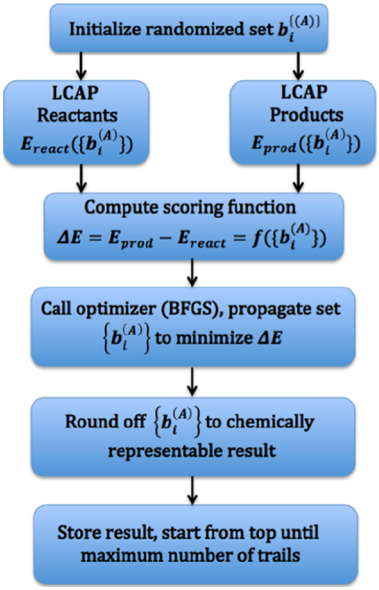

Figure 2. Schematic representation of the ID algorithm based on a scoring function defined by the energy difference between two structures along the catalytic cycle (e.g., the reactant and transition state for the rate-limiting step).

$$k = \frac{k_B T}{h} \exp\left(\frac{-\Delta G^{\ddagger}}{RT}\right) \quad (9)$$

where k_B is the Boltzmann constant, T is the temperature (i.e. 298.15 K), h is Planck's constant, R is the gas constant, and $\Delta G^{\ddagger}$ is the transition state barrier height in kcal/mol.

3. RESULTS AND DISCUSSION

3.1. Inverse Design. Figure 3 shows the synthetically viable options considered for ID as recommended by Crabtree

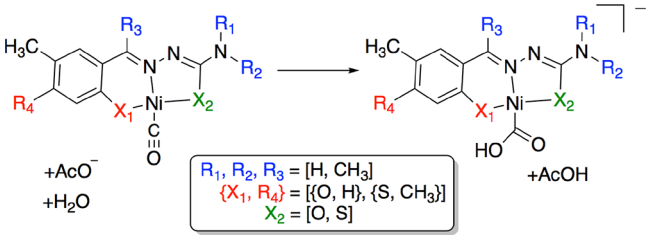

Figure 3. Synthetically viable options considered for ID. The alchemical composition of the individual atomic sites X_i is identical in reactants (left) and products (right) at all times. A total of 32 discrete structures are considered.

and co-workers. In particular, the methyl groups have been placed on several related analogues of the catalyst.[23,24,50] The original ligand is formed via a condensation of a thiosemicarbazide and a hydroxyacetophenone.[24] The differing options at X_1 and X_2 can be generated via commercially available *N*-methylhydrazinecarboxamides/semicarbazides (e.g. CAS: 17696-95-6) and 2′-mercaptoacetophenones (e.g. 26824-02-2) as shown in the Supporting Information. Semicarbazides are soluble in methanol[51] and water[52] (log $P \approx -1.06$) and 2′-mercaptoacetophenone is soluble in ethanol[53] and water (log $P \approx 1.53$)[54,55] suggesting that the alternate ligands would be stable in the experimental methanol/water conditions. The 32 discrete structures span the alchemical

DOI: 10.1021/acs.inorgchem.8b02799
Inorg. Chem. 2018, 57, 15474−15480

potential energy surface on which the LCAP algorithm optimizes the property of interest (i.e., minimum activation energy for the formation of the $[LNi^{II}(COOH)]^-$ intermediate) with respect to the participation coefficients. The participation coefficients $\{b_i^{(A)}\}$ on both sets of structures are initialized with random numbers. Acetate and water molecules are explicitly included in the calculations.

To identify the catalyst yielding the lowest activation energy for the rate-limiting step in the cycle, we initialized 64 calculations starting from random points in the space of participation coefficients $\{b_i^{(A)}\}$. Once a local optimum was identified, the algorithm rounded off the participation coefficients to obtain the closest realistic structure with pure atomic types. After rounding off the 64 local minima, the algorithm produced 21 distinct chemical structures that were subsequently analyzed in terms of their different activation energies, including with DFT. Tables 1 and 2 show the six most frequently found structures (**A**, **B**, **C**, **I**, **J**, and **L**), all of them ranking among the top 12.5%. One of the worst molecules, **D**, was also chosen to be analyzed in Tables 1 and 2, while other structures are given in Table S1.

Table 1. Compositions of Catalyst A, B, C, D, I, J, and L[a]

catalyst	X_1	X_2	R_1	R_2	R_3	R_4
0	O	S	H	CH_3	CH_3	CH_3
A	O	S	H	H	H	H
B	O	O	CH_3	H	CH_3	H
C	O	O	H	H	CH_3	H
D	S	O	H	CH_3	CH_3	CH_3
I	O	O	CH_3	CH_3	H	H
J	O	O	H	H	H	H
L	O	S	H	CH_3	H	H

[a]The labels X_i refer to the atomic positions in Figure 3. The Ni^{II}–iminothiolate catalyst is labeled as 0.

Table 2. Activation Energies in kcal mol for the Catalysts A, B, C, D, I, J, and L (See Figure 3 and Table 1) Found by ID[a]

catalyst	EHT pre	EHT post	DFT
0		26.6	24.2
A	29.3	25.6	23.0
B	29.2	21.3	22.1
C	29.1	22.3	21.9
D	41.6	30.4	24.9
I	29.4	21.2	21.8
J	29.1	22.1	21.6
L	29.5	24.7	23.2

[a]TB (EHT) values before (pre) and after (post) geometry optimization are compared to the DFT (Def2TZVP) energies, after rounding off the participation coefficients. The Ni^{II}–iminothiolate catalyst **0** corresponds to the previously reported complex by Crabtree and co-workers.

Figure 4 shows a representative optimization for member **J** of our sampling, showing that the landscape of the property of interest is smooth as a function of the evolution of participation coefficients.

The energy cost for forming the intermediate $[LNi^{II}COOH]^-$ of the Ni^{II}–iminothiolate catalyst, upon water nucleophilic attack on $[LNi^{II}(CO)]^0$ and subsequent deprotonation, is estimated to be 26.6 kcal/mol according to the TB model Hamiltonian (Table 2), which is higher than the

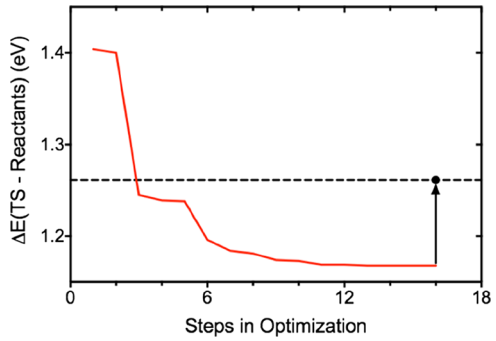

Figure 4. Representative optimization leading to member **J** (shown in Figure 5) of our pool of structures, showing that the landscape for the property of interest is smooth as a function of the evolution of participation coefficients. The black bullet indicates the value of the objective function after rounding off the participation coefficients.

corresponding activation energy obtained for any of the six most frequently found structures (**A**, **B**, **C**, **I**, **J**, and **L**) at the same level of theory (Table 2, second column). The same trend is observed when evaluating the activation energies at the DFT level (Table 2, third column). These results show that the TB description is consistent with DFT and predicts the correct ranking of structures, although the absolute energy values are higher than the corresponding DFT energies, allowing us to do only 7 DFT calculations instead of 42. The parity plot between the methods is provided in the Supporting Information. The lowest activation energy is obtained for catalyst **J** (Figure 5),

Figure 5. Original catalyst **0** before (left) and proposed catalyst **J** after (right) optimization of the reaction energy with the colors matching Figure 3.

with a barrier of 21.6 kcal/mol (i.e., 2.6 kcal/mol lower than that of the original catalyst **0** which corresponds to a turnover frequency higher by 2 orders of magnitude as estimated by transition state theory).

3.2. Catalytic Cycle Featuring the Iminoalkoxylate Catalyst. Figure 6 shows the catalytic cycle (a) and the reaction free energies (b) of the catalytic steps comparing the original iminothiolate complex **0** to the iminoalkoxylate complex **J** found by ID. The energy of **1-TS** is similar for both complexes. The intermediate **2** is more destabilized than **2-TS** when comparing **J** to **0**. The alkoxylate is likely a harder ligand to the soft Ni metal center than the thiolate, thus destabilizing the CO ligand in **2** more than the H_2O ligand in **1** and consequently lowering the energy barrier from 24.1 kcal/mol (close to the estimated barrier based on the rate constants measured by Lu and Crabtree)[23] to 21.6 kcal/mol. Even though the energies of **3** and **4** are slightly increased while the energies of **5** and **6** are slightly decreased when comparing **J** to **0**, none of the steps **3**–**6** involve energy barriers that exceed that of the rate-determining step. The similarities between the free energy profiles suggest that the optimized system **J** shares the same catalytic mechanism as the original one.

The energies of the next highest spin states of steps **1**–**6** of **J** were calculated via DFT and compared to those of their

DOI: 10.1021/acs.inorgchem.8b02799
Inorg. Chem. 2018, 57, 15474–15480

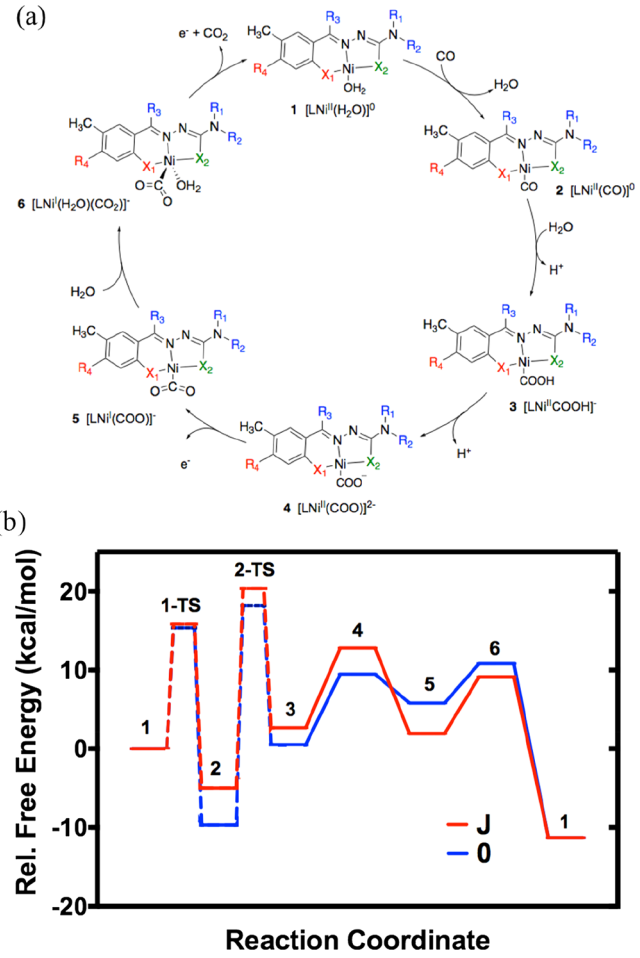

Figure 6. (a) Computed mechanism for the Ni^{II} catalyst. (b) Comparison of the free energy profiles of the original catalyst **0** (blue) and the catalyst **J** found by ID (red). The driving force is provided by the oxidizing agent, mv^{2+}.

corresponding lower spin states. It was found that the higher spin state was always higher in energy and, thus, inaccessible, as displayed in the Supporting Information, just as for the original catalyst.[26]

4. CONCLUSIONS

We introduced an ID scheme to guide the rational design of catalysts based on a TB-LCAP model Hamiltonian. The method requires a reference catalyst with well-defined reaction intermediates and the rate-limiting step of the catalytic process. Molecular candidates with improved performance were searched in the space of alchemical structures defined by synthetically viable changes in the reference complex. The method was illustrated as applied to the search of a Ni^{II} catalyst for CO/CO$_2$ conversion using a biomimetic Ni^{II}–iminothiolate complex as a reference catalyst. The descriptor of catalytic performance was defined in terms of the energy barrier for the rate-limiting step (formation of the [LNi^{II}(COOH)]$^-$ intermediate). The algorithm found a Ni^{II}–iminoalkoxylate analogue complex with improved performance, as defined by the energy barrier of the rate-limiting step (21.6 kcal mol) when compared to the barrier of the reference catalyst (24.1 kcal mol). Similar energies for the other intermediates and transition states along the reaction mechanism showed improved scaling relations. The reported findings demonstrate a valuable tool for catalyst design in larger chemical space that could be readily implemented with any number of descriptors, including not only kinetic barriers but also thermodynamic parameters for reversible reactivity.

■ ASSOCIATED CONTENT

Supporting Information

The Supporting Information is available free of charge on the ACS Publications website at DOI: 10.1021/acs.inorgchem.8b02799.

Compositions of the 21 ID candidates, free energy differences between high and low spin states, proposed synthesis of the designed ligand, additional barrier heights data, and atomic coordinates of optimized geometries for compound **J** (PDF)

■ AUTHOR INFORMATION

Corresponding Author

*E-mail: victor.batista@yale.edu.

ORCID

Benjamin Rudshteyn: 0000-0002-9511-6780

Victor S. Batista: 0000-0002-3262-1237

Notes

The authors declare no competing financial interest.

■ ACKNOWLEDGMENTS

We acknowledge support by the AFOSR grant #FA9550-17-0198 and high performance computing time from NERSC and from the Yale University Faculty of Arts and Sciences High Performance Computing Center, partially funded by the National Science Foundation under grant number CNS08-21132. B.R. gratefully acknowledges support from the NSF Graduate Research Fellowship under grant no. DGE-1122492. The authors thank Prof. Dequan Xiao (University of New Haven) for writing the original version of the ID code. The authors thank Jeffrey Chen and Bob Crabtree (Yale) for suggesting the space of synthetically viable changes in the Ni–iminothiolate complex, and Yueshen Wu for helpful discussions.

■ REFERENCES

(1) Saravanan, K.; Kitchin, J. R.; von Lilienfeld, O. A.; Keith, J. A. Alchemical Predictions for Computational Catalysis: Potential and Limitations. *J. Phys. Chem. Lett.* **2017**, *8*, 5002−5007.

(2) Xiao, D.; Martini, L. A.; Snoeberger, R. C.; Crabtree, R. H.; Batista, V. S. Inverse Design and Synthesis of acac-Coumarin Anchors for Robust TiO_2 Sensitization. *J. Am. Chem. Soc.* **2011**, *133*, 9014−9022.

(3) Franceschetti, A.; Zunger, A. The Inverse Band-Structure Problem of Finding an Atomic Configuration With Given Electronic Properties. *Nature* **1999**, *402*, 60−63.

(4) Hu, X.; Hu, H.; Beratan, D. N.; Yang, W. A Gradient-Directed Monte Carlo Approach for Protein Design. *J. Comput. Chem.* **2010**, *31*, 2164−2168.

(5) von Lilienfeld, O. A.; Lins, R. D.; Rothlisberger, U. Variational Particle Number Approach for Rational Compound Design. *Phys. Rev. Lett.* **2005**, *95*, 153002.

(6) Wang, M.; Hu, X.; Beratan, D. N.; Yang, W. Designing Molecules by Optimizing Potentials. *J. Am. Chem. Soc.* **2006**, *128*, 3228−3232.

(7) von Lilienfeld, O. A. Accurate ab initio Energy Gradients in Chemical Compound Space. *J. Chem. Phys.* **2009**, *131*, 164102.

DOI: 10.1021/acs.inorgchem.8b02799
Inorg. Chem. 2018, 57, 15474−15480

(8) Weymuth, T.; Reiher, M. Inverse Quantum Chemistry: Concepts and Strategies for Rational Compound Design. *Int. J. Quantum Chem.* **2014**, *114*, 823−837.
(9) Sanchez-Lengeling, B.; Aspuru-Guzik, A. Inverse Molecular Design Using Machine Learning: Generative Models for Matter Engineering. *Science* **2018**, *361*, 360−365.
(10) Weymuth, T.; Reiher, M. Gradient-Driven Molecule Construction: An Inverse Approach Applied to the Design of Small-Molecule Fixating Catalysts. *Int. J. Quantum Chem.* **2014**, *114*, 838−850.
(11) Dittner, M.; Hartke, B. Globally Optimal Catalytic Fields—Inverse Design of Abstract Embeddings for Maximum Reaction Rate Acceleration. *J. Chem. Theory Comput.* **2018**, *14*, 3547−3564.
(12) Huwig, K.; Fan, C.; Springborg, M. From Properties to Materials: An Efficient and Simple Approach. *J. Chem. Phys.* **2017**, *147*, 234105.
(13) Dudiy, S. V.; Zunger, A. Searching for Alloy Configurations with Target Physical Properties: Impurity Design via a Genetic Algorithm Inverse Band Structure Approach. *Phys. Rev. Lett.* **2006**, *97*, 046401.
(14) Piquini, P.; Graf, P. A.; Zunger, A. Band-Gap Design of Quaternary (In, Ga)(As, Sb) Semiconductors via the Inverse-Band-Structure Approach. *Phys. Rev. Lett.* **2008**, *100*, 186403.
(15) Xiao, D.; Yang, W.; Beratan, D. N. Inverse Molecular Design in a Tight-Binding Framework. *J. Chem. Phys.* **2008**, *129*, 044106.
(16) Hu, X.; Beratan, D. N.; Yang, W. A Gradient-Directed Monte Carlo Approach to Molecular Design. *J. Chem. Phys.* **2008**, *129*, 064102.
(17) Keinan, S.; Hu, X.; Beratan, D. N.; Yang, W. Designing Molecules with Optimal Properties Using the Linear Combination of Atomic Potentials Approach in an AM1 Semiempirical Framework. *J. Phys. Chem. A* **2007**, *111*, 176−181.
(18) Hu, X.; Beratan, D. N.; Yang, W. A Gradient-Directed Monte Carlo Method for Global Optimization in a Discrete Space: Application to Protein Sequence Design and Folding. *J. Chem. Phys.* **2009**, *131*, 154117.
(19) Evans, D. J. Chemistry Relating to the Nickel Enzymes CODH and ACS. *Coord. Chem. Rev.* **2005**, *249*, 1582−1595.
(20) Lindahl, P. A. The Ni-Containing Carbon Monoxide Dehydrogenase Family: Light at the End of the Tunnel? *Biochemistry* **2002**, *41*, 2097−2105.
(21) Qiu, D.; Kumar, M.; Ragsdale, S. W.; Spiro, T. G. Nature's Carbonylation Catalyst: Raman Spectroscopic Evidence That Carbon Monoxide Binds to Iron, Not Nickel, in CO Dehydrogenase. *Science* **1994**, *264*, 817−819.
(22) Shin, W.; Lindahl, P. A. Discovery of a Labile Nickel Ion Required for CO/Acetyl-CoA Exchange Activity in the NiFe Complex of Carbon Monoxide Dehydrogenase From Clostridium thermoaceticum. *J. Am. Chem. Soc.* **1992**, *114*, 9718−9719.
(23) Lu, Z.; Crabtree, R. H. A Functional Modeling Study of the CO Oxidation Site of Nickel CO Dehydrogenase. *J. Am. Chem. Soc.* **1995**, *117*, 3994−3998.
(24) Lu, Z.; White, C.; Rheingold, A. L.; Crabtree, R. H. Functional Modeling of CO Dehydrogenase: Catalytic Reduction of Methylviologen by CO/H_2O with an N, O, S-Ligated Nickel Catalyst. *Angew. Chem., Int. Ed.* **1993**, *32*, 92−94.
(25) Stavropoulos, P.; Muetterties, M. C.; Carrie, M.; Holm, R. H. Structural and Reaction Chemistry of Nickel Complexes in Relation to Carbon Monoxide Dehydrogenase: A Reaction System Simulating Acetyl-Coenzyme a Synthase Activity. *J. Am. Chem. Soc.* **1991**, *113*, 8485−8492.
(26) Wu, Y.; Rudshteyn, B.; Warnke, I.; Xiao, D.; Batista, V. S. Mechanistic Study of CO/CO_2 Conversion Catalyzed by a Biomimetic Ni(II)-Iminothiolate Complex. *Int. J. Quantum Chem.* **2017**, *118*, No. e25555.
(27) Burdett, J. K. *Chemical Bonding in Solids*; Oxford University Press, 1995.
(28) Hoffmann, R. A Chemical and Theoretical Way to Look at Bonding on Surfaces. *Rev. Mod. Phys.* **1988**, *60*, 601−628.
(29) Abuabara, S. G.; Rego, L. G. C.; Batista, V. S. Influence of Thermal Fluctuations on Interfacial Electron Transfer in Functionalized TiO_2 Semiconductors. *J. Am. Chem. Soc.* **2005**, *127*, 18234−18242.
(30) Rego, L. G. C.; Abuabara, S. G.; Batista, V. S. Model Study of Coherent Quantum Dynamics of Hole States in Functionalized Semiconductor Nanostructures. *J. Chem. Phys.* **2005**, *122*, 154709.
(31) Rego, L. G. C.; Batista, V. S. Quantum Dynamics Simulations of Interfacial Electron Transfer in Sensitized TiO_2 Semiconductors. *J. Am. Chem. Soc.* **2003**, *125*, 7989−7997.
(32) McNamara, W. R.; Snoeberger, R. C.; Li, G.; Schleicher, J. M.; Cady, C. W.; Poyatos, M.; Schmuttenmaer, C. A.; Crabtree, R. H.; Brudvig, G. W.; Batista, V. S. Acetylacetonate Anchors for Robust Functionalization of TiO_2 Nanoparticles with Mn(II)-Terpyridine Complexes. *J. Am. Chem. Soc.* **2008**, *130*, 14329−14338.
(33) Abuabara, S. G.; Cady, C. W.; Baxter, J. B.; Schmuttenmaer, C. A.; Crabtree, R. H.; Brudvig, G. W.; Batista, V. S. Ultrafast Photooxidation of Mn (II)−Terpyridine Complexes Covalently Attached to TiO_2 Nanoparticles. *J. Phys. Chem. C* **2007**, *111*, 11982−11990.
(34) Ammeter, J. H.; Bürgi, H. B.; Thibeault, J. C.; Hoffmann, R. Counterintuitive Orbital Mixing in Semiempirical and ab initio Molecular Orbital Calculations. *J. Am. Chem. Soc.* **1978**, *100*, 3686−3692.
(35) Parr, R. G.; Yang, W. *Density-Functional Theory of Atoms and Molecules*; Oxford University Press: New York, 1989.
(36) Kohn, W.; Sham, L. J. Self-Consistent Equations Including Exchange and Correlation Effects. *Phys. Rev.* **1965**, *140*, A1133−A1138.
(37) Hohenberg, P.; Kohn, W. Inhomogeneous Electron Gas. *Phys. Rev.* **1964**, *136*, B864−B871.
(38) Becke, A. D. Density-Functional Thermochemistry. III. The Role of Exact Exchange. *J. Chem. Phys.* **1992**, *98*, 5648−5652.
(39) Lee, C.; Yang, W.; Parr, R. G. Development of the Colle-Salvetti Correlation-Energy Formula Into a Functional of the Electron Density. *Phys. Rev. B: Condens. Matter Mater. Phys.* **1988**, *37*, 785−789.
(40) Frisch, M. J. T.; Trucks, G. W.; Schlegel, H. B.; Scuseria, G. E.; Robb, M. A.; Cheeseman, J. R.; Scalmani, G.; Barone, V.; Mennucci, B.; Petersson, G. A.; Nakatsuji, H.; Caricato, M.; Li, X.; Hratchian, H. P.; Izmaylov, A. F.; Bloino, J.; Zheng, G.; Sonnenberg, J. L.; Hada, M.; Ehara, M.; Toyota, K.; Fukuda, R.; Hasegawa, J.; Ishida, M.; Nakajima, T.; Honda, Y.; Kitao, O.; Nakai, H.; Vreven, T.; Montgomery, J. A., Jr.; Peralta, J. E.; Ogliaro, F.; Bearpark, M.; Heyd, J. J.; Brothers, E.; Kudin, K. N.; Staroverov, V. N.; Kobayashi, R.; Normand, J.; Raghavachari, K.; Rendell, A.; Burant, J. C.; Iyengar, S. S.; Tomasi, J.; Cossi, M.; Rega, N.; Millam, N. J.; Klene, M.; Knox, J. E.; Cross, J. B.; Bakken, V.; Adamo, C.; Jaramillo, J.; Gomperts, R.; Stratmann, R. E.; Yazyev, O.; Austin, A. J.; Cammi, R.; Pomelli, C.; Ochterski, J. W.; Martin, R. L.; Morokuma, K.; Zakrzewski, V. G.; Voth, G. A.; Salvador, P.; Dannenberg, J. J.; Dapprich, S.; Daniels, A. D.; Farkas, Ö.; Foresman, J. B.; Ortiz, J. V.; Cioslowski, J.; Fox, D. J. *Gaussian 09*, Rev. D; Gaussian, Inc.: Wallingford CT, 2009.
(41) Cramer, C. J. *Essentials of Computational Chemistry: Theories and Models*; John Wiley & Sons: West Sussex, England, 2004; pp 355−383.
(42) Weigend, F.; Ahlrichs, R. Balanced Basis Sets of Split Valence, Triple Zeta Valence and Quadruple Zeta Valence Quality for H to Rn: Design and Assessment of Accuracy. *Phys. Chem. Chem. Phys.* **2005**, *7*, 3297−3305.
(43) Hehre, W. J.; Ditchfield, R.; Pople, J. A. Self-Consistent Molecular Orbital Methods. XII. Further Extensions of Gaussian-Type Basis Sets for Use in Molecular Orbital Studies of Organic Molecules. *J. Chem. Phys.* **1972**, *56*, 2257−2261.
(44) Clark, T.; Chandrasekhar, J.; Spitznagel, G. W.; Schleyer, P. V. R. Efficient Diffuse Function-Augmented Basis Sets for Anion Calculations. III. The 3-21+G Basis Set for First-Row Elements, Li-F. *J. Comput. Chem.* **1983**, *4*, 294−301.

DOI: 10.1021/acs.inorgchem.8b02799
Inorg. Chem. 2018, 57, 15474−15480

(45) Krishnan, R.; Binkley, J. S.; Seeger, R.; Pople, J. A. Self-Consistent Molecular Orbital Methods. XX. A Basis Set for Correlated Wave Functions. *J. Chem. Phys.* **1980**, *72*, 650−654.
(46) Marenich, A. V.; Cramer, C. J.; Truhlar, D. G. Universal Solvation Model Based on Solute Electron Density and on a Continuum Model of the Solvent Defined by the Bulk Dielectric Constant and Atomic Surface Tensions. *J. Phys. Chem. B* **2009**, *113*, 6378−6396.
(47) Keith, J. A.; Carter, E. A. Quantum Chemical Benchmarking, Validation, and Prediction of Acidity Constants for Substituted Pyridinium Ions and Pyridinyl Radicals. *J. Chem. Theory Comput.* **2012**, *8*, 3187−3206.
(48) Clark, M. L.; Cheung, P. L.; Lessio, M.; Carter, E. A.; Kubiak, C. P. Kinetic and Mechanistic Effects of Bipyridine (bpy) Substituent, Labile Ligand, and Brønsted Acid on Electrocatalytic CO_2 Reduction by Re (bpy) Complexes. *ACS Catal.* **2018**, *8*, 2021−2029.
(49) Arrhenius, S. Über die Reaktionsgeschwindigkeit bei der Inversion von Rohrzucker durch Säuren. *Z. Phys. Chem.* **1889**, *4U*, 226.
(50) Lu, Z.; White, C.; Rheingold, A. L.; Crabtree, R. H. Deprotonated Thioamides as Thiolate S-Donor Ligands With a High Tendency to Avoid M-S-M Bridge Formation: Crystal and Molecular Structure of Bis(2-Hydroxy-5-Methylacetophenone N,N-Dimethylthiosemicarbazonato)Dinickel. *Inorg. Chem.* **1993**, *32*, 3991−3994.
(51) Rothgery, E. F. Process for Preparing Semicarbazide Hydrochloride. U.S. Patent 4,482,738 A, Nov 13, 1984.
(52) Haller, H. L.; LaForge, F. B. A Crystalline Compound of Semicarbazide and Semicarbazide Hydrochloride. *J. Am. Chem. Soc.* **1937**, *59*, 760.
(53) Hiskey, R. G.; Kepler, J. A.; Thomas, B. D. Chemistry of Aliphatic Disulfides. X. Studies on the Mechanism of the Alkoxide Cleavage of 1,6-Diphenyl-3,4-dithia-1,6-hexanedione1,2. *J. Org. Chem.* **1964**, *29*, 3684−3687.
(54) Petrauskas, A. A.; Kolovanov, E. A. ACD/Log P Method Description. *Perspect. Drug Discovery Des.* **2000**, *19*, 99−116.
(55) *ChemDraw Professional, 17*; CambridgeSoft, 2017.

DOI: 10.1021/acs.inorgchem.8b02799
Inorg. Chem. 2018, 57, 15474−15480